



HAL
open science

Compelling Evidence for the Role of Retained Austenite in the Formation of Low Cycle Fatigue Extrusions in a 9Ni Steel

Mahira Cota Araujo, Jean-Marc Olive, Gilles Pecastaings, Ahmed Addad, Jérémie Bouquerel, Jean-Bernard Vogt

► To cite this version:

Mahira Cota Araujo, Jean-Marc Olive, Gilles Pecastaings, Ahmed Addad, Jérémie Bouquerel, et al.. Compelling Evidence for the Role of Retained Austenite in the Formation of Low Cycle Fatigue Extrusions in a 9Ni Steel. *Metals*, 2023, 13 (3), pp.546. 10.3390/met13030546 . hal-04309189

HAL Id: hal-04309189

<https://hal.science/hal-04309189>

Submitted on 27 Nov 2023

HAL is a multi-disciplinary open access archive for the deposit and dissemination of scientific research documents, whether they are published or not. The documents may come from teaching and research institutions in France or abroad, or from public or private research centers.

L'archive ouverte pluridisciplinaire **HAL**, est destinée au dépôt et à la diffusion de documents scientifiques de niveau recherche, publiés ou non, émanant des établissements d'enseignement et de recherche français ou étrangers, des laboratoires publics ou privés.



Distributed under a Creative Commons Attribution 4.0 International License

Article

Compelling Evidence for the Role of Retained Austenite in the Formation of Low Cycle Fatigue Extrusions in a 9Ni Steel

Mahira A. Cota Araujo^{1,2}, Jean-Marc Olive³, Gilles Pecaistaings⁴, Ahmed Addad¹, Jérémie Bouquerel¹ 
and Jean-Bernard Vogt^{1,*} 

¹ CNRS, INRAE, Centrale Lille, UMR 8207—UMET—Unité Matériaux et Transformations, Université de Lille, 59000 Lille, France; mahira.araujo@gmail.com (M.A.C.A.); ahmed.addad@univ-lille.fr (A.A.); jeremie.bouquerel@centralelille.fr (J.B.)

² Villares Metals, SA. Sumaré, São Paulo 13178-902, Brazil

³ CNRS, Institut de Mécanique et d'Ingénierie, UMR 5295, Université de Bordeaux, 33405 Talence, France; jean-marc.olive@u-bordeaux.fr

⁴ Centre de Recherche Paul Pascal, UMR 5031 CNRS, Université de Bordeaux, 33600 Pessac, France; gilles.pecastaings@crpp.cnrs.fr

* Correspondence: jean-bernard.vogt@centralelille.fr

Abstract: The 9Ni martensitic steels have a martensitic microstructure which contains retained austenite after solution heat treatment and water quenching. Under low cycle fatigue, extrusions formed at the surface of the material and were very close to martensite lath boundaries. The presence of retained austenite at martensite laths has been highly suspected to impact the cyclic plasticity. However, the nano-size of the austenitic phase makes it difficult to obtain clear evidence of its role. The paper focuses on the precise determination of these extrusions and the link with the retained austenite. The paper also emphasizes the innovative and promising use of magnetic force microscopy (MFM) to document cyclic plasticity of a 9Ni steel. It is shown that electron microscopies, even the most advanced ones, may be unsuccessful in reaching this goal, while magnetic force microscopy (MFM) overcame the difficulty. This technique has allowed imaging of both the extrusion and the retained austenite. These analyses confirm that the fatigue extrusions originated from a local displacement of martensite lath. The proposed mechanism, in which the retained austenitic film acts as a lubricant film or greasy film promoting a flowing of martensite along the interfaces, is unambiguously demonstrated.

Keywords: martensite; cyclic plasticity; magnetic force microscopy; advanced electron microscopy



Citation: Cota Araujo, M.A.; Olive, J.-M.; Pecaistaings, G.; Addad, A.; Bouquerel, J.; Vogt, J.-B. Compelling Evidence for the Role of Retained Austenite in the Formation of Low Cycle Fatigue Extrusions in a 9Ni Steel. *Metals* **2023**, *13*, 546. <https://doi.org/10.3390/met13030546>

Academic Editor:

Alireza Akhavan-Safar

Received: 9 February 2023

Revised: 1 March 2023

Accepted: 6 March 2023

Published: 8 March 2023



Copyright: © 2023 by the authors. Licensee MDPI, Basel, Switzerland. This article is an open access article distributed under the terms and conditions of the Creative Commons Attribution (CC BY) license (<https://creativecommons.org/licenses/by/4.0/>).

1. Introduction

Fatigue is the most frequent fracture cause of engineering components. It results from repeated loading and unloading, and certain amplitudes lead to different domains of fatigue, from ultra-low and low cycle fatigue (LCF) to high and very high cycle fatigue (VHCF). The main difference between them is whether the material is cyclically loaded over or under the yield stress, respectively. When a metal is cyclically loaded in the LCF regime, it becomes entirely plastically deformed. When the working temperature is less than a third of the melting temperature, the cyclic deformation is, most of time, accommodated by movement of dislocations and sometimes by twinning or phase transformation. The localization of the cyclic plastic deformation in the so-called persistent slip bands (PSBs) is one of the characteristics of fatigue damage. Since the 1970s and 1980s, considerable efforts have been made to understand the formation of PSBs, and a clear link between PSBs and microcracks nucleation was pointed out on nickel or copper, e.g., [1–6]. The ladder-like featured PSBs, which concentrate the irreversible plastic deformation, emerge at the external surface. The interactions between the moving dislocations in the PSBs also result in point defects production, e.g., [7–9]. The sharpness of the slip mark pattern formed at the surface

evolves with the number of cycles and is later accompanied by depressions, giving rise to the well-known extrusion–intrusion pairs. Additionally, there has been considerable effort made to understand the formation of extrusions and intrusions, since it has been shown that intrusions are the embryo for short fatigue cracks. It is clear that the developments of the methodologies and the selected imaging tools are determined for pointing out the link between intrusions, microcracks, and extrusions. By using careful interferometry, Cheng and Laird [10] showed that the emerged PSBs had a certain distribution of slip offsets. The PSB which was the narrowest and possessed the greatest slip offset was the preferred site of crack nucleation. Atomic force microscopy (AFM) is a high-resolution non-optical imaging technique suitable for visualizing the relief of a surface and for measuring the roughness. It has been employed for the study of the evolution of the roughness induced by cyclic loading with the number of cycles without the destruction of the sample, e.g., [3,11,12]. The intent to image both the intrusion and extrusion has motivated dedicated experiments. This is a huge problem since the observations of the surface relief by scanning electron microscopy (SEM) or atomic force microscopy (AFM) alone have rapidly been confronted with the problem of imaging the intrusions which grow in the bulk and the extrusion which can exhibit different shapes such as the curved one. To overcome these limitations, the sharp-corner technique coupled with SEM [13] or the replica technique [14] allowed the imaging of PSB and crack initiation along the PSB in copper single crystal. More recently, the focused ion beam (FIB) technique was employed by, e.g., [15,16] to extract, by ion milling, cross section lamella which was further observed by transmission electron microscopy (TEM). This allows revealing the real shape of extrusion and the precise location and depth of the intrusion or microcrack. Based on this experimental evidence of single and polycrystalline, pure or solution alloyed annealed metals, such as copper or 316 L austenitic stainless steel, different models for extrusion–intrusion pairs have been proposed, e.g., [17–20]. The latter authors have been intensively refining their concept. They confirmed and emphasized the role of PSB embedded in a quasi-elastic matrix, the interactions between dislocations in the PSB, the production of vacancies, and their migration at the interface between PSB and matrix. Polak et al. [21] also showed that this physical concept is valid for other structural materials such as Sanicro 25 where the dislocation slip mode is planar instead of wavy.

It is paradoxical to believe that the analysis of extrusion–intrusion network still remains challenging. Indeed, the performances of the surface analysis tools are continuously increasing, especially in terms of resolution. However, at the same time, the complexity of the microstructure of some engineering materials diverges from “simple” microstructure materials, as, for example, austenitic or ferritic stainless steels. This is the case of bainitic, martensitic, or pearlitic steels which are characterized by a hierarchical microstructure. This means that the microstructure can be described at different structural units of varying length scales. For martensitic steels, these are lath, sub-block, block, packet, and prior-austenite grains. It is justified to raise the question of whether extrusions and intrusions form with a similar feature as for the simple microstructure materials previously mentioned. Despite this, extrusions form with morphologies similar to those in simple microstructure metals [22–24]. In a 12Cr (fully) martensitic steel subjected to LCF at room temperature, Seidametova et al. [24] have shown that cyclic plasticity events occur at the scale of the martensite lath, where dislocations can glide more or less easily from considerable distances within them, depending on the metallurgical state of the material and the applied stress. Therefore, dislocation glide can remain confined to martensite laths, leading to intensive slip band or dislocation cells, and sometimes to lath coarsening. Though the classical ladder like PSBs were not observed, we have recently proposed that the martensite laths play the same role as PSBs, and additionally, the interfaces between laths are comparable to those between PSB and the matrix found in copper or 316 L. As a result, extrusions formed in the middle of the laths while intrusions formed at martensite lath interfaces, which validated the analogy between a lath interface in the martensitic steel with a PSB/matrix interface in large grain single phased metals [24]. The 9Ni quenched steel also exhibits the hierarchical microstructure but contains, in addition, retained austenite along the lath boundaries. After

low cycle fatigue tests conducted similarly as for the 12Cr steel, the opposite situation was observed. Intrusions were observed in the middle of the laths and extrusions in the vicinity of lath interfaces [25]. It was then concluded that, in the 9Ni martensitic steel, the extrusions were the result of the deformation of the laths which was aided by the retained austenite at the lath boundaries. The latter was considered to act only as a lubricant facilitating the martensite displacement along the interfaces [25]. This explanation is fully acceptable and fits well the proposed role of nano-films of retained austenite which act like greasy plane on which stiffer body-centered cubic (BCC) laths can slide [26]. Nevertheless, the retained austenite associated with the extrusion network was not sufficiently clearly and unambiguously evidenced, giving rise to possible discussion of the mechanism. To strengthen our concept, additional microstructural investigations appeared necessary. However, revealing the exact location of retained austenite together with the position of the extrusion is challenging because of the sharpness of the microstructural elements. Moreover, as the retained austenite is a metastable phase, it can even transform under sample preparation.

The objective of the present paper is to definitively and ambiguously demonstrate the precise location of fatigue extrusions together with the austenite films. It also aims at pointing out the overcoming of difficulties of imaging nanosized lamella of austenite in a martensitic matrix. Finally, the paper also shows the successful outcome of using a complementarity of topography analysis techniques with the physical properties (magnetic properties) tools for understanding the role of the microstructure of complex microstructure materials in cyclic plasticity.

2. Material and Methods

2.1. Material and Conventional Techniques for Microstructure Identification

The steel considered in the present study was provided by Salzgitter Mannesmann, Saint-Mande, France and contains (in wt.%) 0.04 C, 8.99 Ni, 0.53 Mn, 0.23 Si. The sample was austenitized at 900 °C and then quenched in water.

X-ray diffraction (XRD) was employed for identification of crystallographic phases and their volume fraction measurement. For that purpose, the Rigaku Smartlab Diffractometer (Rigaku corporation, Tokyo, Japan) equipped with a copper source ($\lambda = 1.54056 \text{ \AA}$) operated in a 2θ range between 38 and 120° was employed. The diffractograms were then treated to estimate the volume fraction of austenite before and after fatigue by considering the Cullity method [27]. This method considers the intensity of the (200), (211), (220), and (311) peaks of austenite. Then, the austenite fraction is obtained with Equation (1):

$$fy = \frac{1}{4} \left(\frac{I_{\gamma}^{220}}{1.42 * I_{\alpha}^{200} + I_{\gamma}^{220}} + \frac{I_{\gamma}^{220}}{0.71 * I_{\alpha}^{211} + I_{\gamma}^{220}} + \frac{I_{\gamma}^{311}}{1.62 * I_{\alpha}^{200} + I_{\gamma}^{311}} + \frac{I_{\gamma}^{311}}{0.81 * I_{\alpha}^{211} + I_{\gamma}^{311}} \right) \quad (1)$$

The (110) and (111) peaks are not considered for this calculation because they can lead to some uncertainties as they are too close to each other in the diffractogram.

To highlight the location of austenite inside the ferritic matrix, several conventional techniques were employed. At first, the microstructure was first investigated by Light Optical Microscopy (LOM), Scanning Electron Microscopy (SEM) in the secondary electrons mode, Electron Backscatter Diffraction (SEM-EBSD), and Transmission Electron Microscopy (TEM). The observations of the microstructure at the prior austenitic grain size scale were performed after classical polishing and etching. The surface preparation consisted of a mechanical polishing first with SiC paper and then with diamond paste up to 1 μm granulometry. Finally, the material was chemically etched with Nital 3% solution. For the SEM-EBSD analysis, a fine-polishing step with Struers OP-U 0.04 μm colloidal silica suspension (Struers, Rødovre, Denmark) was added to obtain a proper smooth surface. The SEM equipment was a Hitachi SU-5000 FEG-SEM system (Hitachi, Tokyo, Japan) operated at 20 kV with an Oxford Instruments® EBSD system (Abington, UK) with a minimum angular resolution of 0.5° and by selecting a scan step size of 100 nm. The observations at

the martensite lath scale by TEM required preparation of thin foils. For that, sheets were cut from the material block parallel to the rolling direction, mechanically ground, and thinned up to 80 μm . Then, 3 mm disks were extracted and subsequently thinned with the Struers Tenupol double jet polisher using a solution of 90% acetic acid and 10% perchloric acid at 12 °C and 20.5 V of applied tension. Finally, the thin foils were afterward cleaned using a Gatan (Gatan, Inc., Pleasanton, CA, USA) Precision Ion Beam Polishing (PIPS). The FEI Tecnai G2-20 twin TEM (FEI, Hillsboro, OR, USA) operating at 200 kV was employed for imaging the microstructure together with diffraction. More advanced techniques have been also employed and will be introduced later in the article.

2.2. Fatigue Testing

Flat LCF specimens were cut according to ASTM E606 by spark erosion. The specimens had a gauge length of 12 mm and a cross-section of 6 mm \times 3 mm. The gauge part was prepared by mechanical polishing and finished with a $\frac{1}{4}$ μm diamond paste. Additionally, a fine-polishing step with Struers OP-U 0.04 μm colloidal silica suspension was performed to obtain a proper smooth surface for post-deformation analysis. Based on previous results, the material was cycled at room temperature under total strain control $\Delta\epsilon_t = 1.2\%$ for 80 cycles, which represented 5% of the fatigue life. Strain was measured by means of a strain gauge extensometer (MTS model 632.26F-30, MTS Corp., Minneapolis, MN, USA) of 8 mm gauge length directly attached onto the gauge part of the specimen. The strain signal was triangular with a strain ratio $R_\epsilon = -1$ and a constant strain rate of $4 \times 10^{-3} \text{ s}^{-1}$.

3. Results and Discussion

3.1. Preliminary Results

Figure 1 shows the LOM image of the microstructure of the material. The classical hierarchical martensitic microstructure comprises an average prior austenitic grain size of 14 μm , a packet size of 5 μm , and a block size of 3 μm . A more detailed description can be found in [25]. Though XRD analysis pointed out both the ferritic BCC phase and the austenitic FCC one, the retained austenite cannot be revealed by LOM or SEM because it might be in the form of very small crystals, confirmed by TEM as reported in the literature [26,28] and later on identified (see Section 3.3). Based on the Cullity method, the austenite content was estimated to be between 8 and 10%.

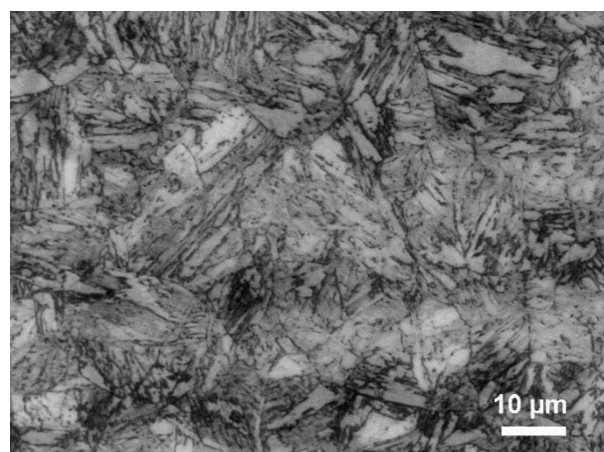


Figure 1. Light optical image showing the martensitic structure of the quenched 9Ni steel. Reprinted with permission from ref. [25]. Copyright 2021 Elsevier.

Cycling the material under a total strain range $\Delta\epsilon_t = 1.2\%$ required applying an increasing stress up to about 10 cycles which then decreased with the further cycles. This stress response to strain cycling refers to a cyclic hardening followed by continuous softening. This behavior is very typical of martensitic steels and mainly depends on the applied strain range and temperature [29,30]. In this family of steels, the plastic strain is

accommodated by the gliding of the preexisting dislocations inside the martensite laths (see Figure 6a) and sometimes involves lath coalescence. For the studied steel of this paper, a possible transformation of the retained austenite was also considered. Nevertheless, the amount of austenite quantified after 650 cycles (fatigue life) by XRD was found to be slightly lower (5%), suggesting that the TRIP (transformation induced plasticity) effect did not control the cyclic plasticity. The strain accommodation was revealed by the presence of a well-formed extrusions network accompanied by intrusions and easily formed, as can be seen in Figure 2. This 2D image reveals the curved shape of the extrusion, which sometimes makes the identification of the neighboring intrusion impossible, depending on its location side. Extrusions are near the interface of the martensite lath but it is impossible to conclude whether the extruded matter is austenite or martensite.

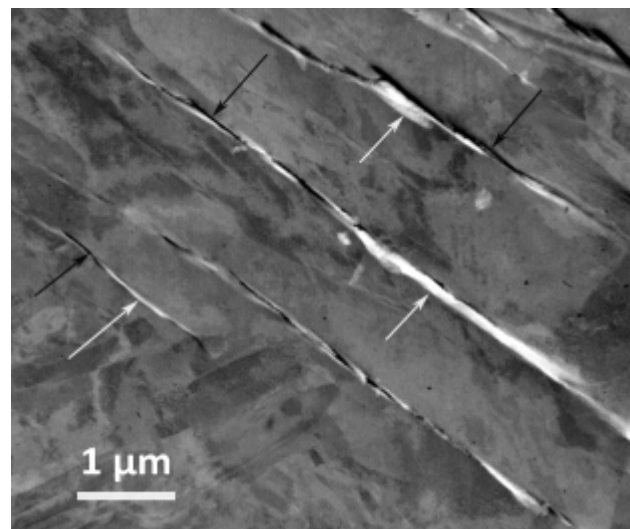


Figure 2. SEM image showing extrusions (white arrows) and intrusions (black arrows) at the surface of the quenched 9Ni steel after 80 cycles at $\Delta\epsilon_t = 1.2\%$.

3.2. Link between Fatigue Extrusion and Microstructure Revealed by TEM

To overcome this limitation, cross-section by using the focused-ion beam technique (FIB) was performed for imaging the extrusion–intrusion pairs in relation to the retained austenite. Cross-sectional lamellas were extracted from selected zones covered by extrusion–intrusion pairs using the dual beam workstation FEI Quanta 3D (FEI, Hillsboro, OR, USA). The area of interest was covered by two different layers in order to protect the surface against ion insertion: a thin layer of carbon deposited by electron bombardment and a thick layer of platinum (about 1 μm) sputtered by ion bombardment. Firstly, a coarse FIB machining with a current of 20 nA and a tension of 30 kV formed the craters from both sides of the future lamella. Then the lamella was cut and transported on a copper grid and again thinned with a low ion energy beam (5 keV) and a weaker current of 100 pA in order to remove or minimize the damage caused by the previous steps.

The FIB-thinned lamellae were then observed by high-resolution transmission electron microscopy (HRTEM) in a FEI TITAN Themis 300 microscope (FEI, Hillsboro, OR, USA). This allowed the appreciation of the real shape of the extrusions and their location, next to the martensite lath boundaries (Figure 3a). However, the austenite film was not revealed as a detrimental effect of the FIB technique, which can transform the austenite into martensite depending on the stability of the austenite [31].

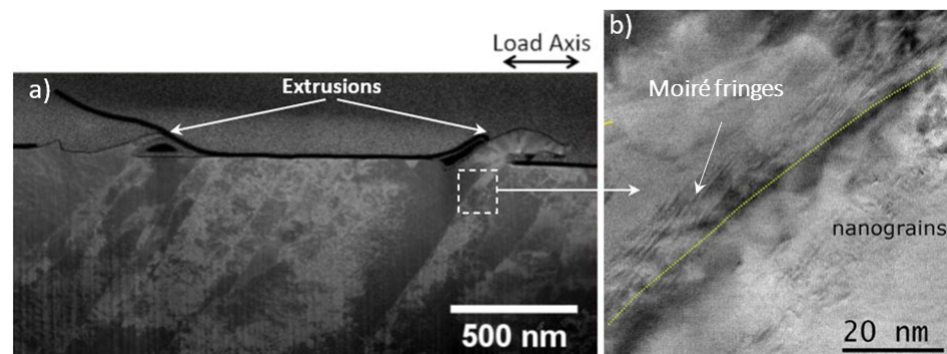


Figure 3. (a) HRTEM image of extrusions after 80 cycles at $\Delta\epsilon_t = 1.2\%$ located at lath interfaces and (b) Moiré fringes at the lath boundary underlined by the yellow dashed line.

To claim their initial presence before the preparation of the lamellae, deep attention has been paid to this area. Figure 3b is a bright-field micrograph closer to the extrusion zone pointing out fringes near the boundary. These fringes are typical Moiré fringes, as may occur in optics when two patterns of line grids on screens are superposed on each other and slightly inclined to one another. Moiré fringes can also be observed in SEM or in TEM. They are formed by the optical-like projection of transmitted electron beams owing to superimposed crystal lattices in the beam path. Moiré fringe processing is useful for qualitative analysis of defect and strain in SEM or TEM or for evaluation of epitaxial films grown on a substrate [32]. In the present study, they can reflect the presence of two phases since they are formed when two (or more) crystal lattices are interfered with, caused by a misfit between the lattice parameter of two phases. Those interference fringes were already noticed at the austenitic/martensitic interface in 9Ni steel, representing a small mismatch between the $(111)\gamma$ and $(110)\alpha$ parallel planes [33]. This tends to support that a remaining portion of the austenite is still present but was not in sufficient quantity to obtain a clear diffraction pattern.

To find additional indicators of the former presence of austenite, another extrusion placed at the boundary (Figure 4a) was analyzed in terms of chemical composition mapping (Figure 4b). Close attention paid to the carbon distribution reveals a higher concentration of this element at the interface (Figure 4b).

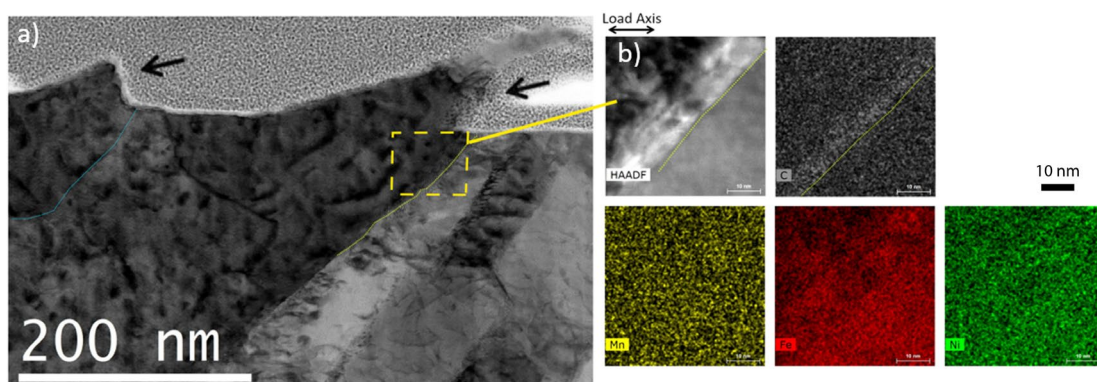


Figure 4. (a) HRTEM images of extrusion after 80 cycles at $\Delta\epsilon_t = 1.2\%$ located and (b) EDX mapping at the lath boundary underlined in the area delimited by the yellow dashed line.

Atom probe investigations performed by Morito et al. [28] showed a significant change in the carbon content at the interface due to the presence of the very thin austenitic films in as-quenched martensitic steels. This might lead to the conclusion that the identified carbon enrichment is linked to the former austenite film that existed at the interface and was transformed by the FIB machining.

3.3. Clear Assessment of the Nature of Fatigue Extrusion and of the Link with Retained Austenite by MFM

Based on HRTEM analysis of FIB-thinned lamellae, there is a strong presumption that an austenite film is present between the martensite interface and the extrusion. However, an accumulation of clues does not make a proof. The next set of experiments based on magnetic force microscopy (MFM) aimed at providing proof of the presence of the austenite distributed at the interface and, therefore, consolidating the role played by this phase in the accommodation of plastic deformation together with the location of extrusion. MFM is a variant of an atomic force microscopy where the scanning tip is coated with ferromagnetic material. The tip scans the surface, detects, and displays as images the stray fields present on the surface of the sample. Thus, it allows the acquisition of images reflecting the local magnetic properties of the sample surface at the nanoscale. MFM found many applications ranging from electronic engineering and physics to biological and biomedical engineering [34,35]. It has also been already employed in metallurgy to differentiate austenite from ferrite, e.g., in a duplex steel or in a transformation induced plasticity (TRIP) steel [36,37]. MFM was also successful to elucidate the micro-mechanisms of plastic deformation in metallic glasses [38]. However, for the duplex steel or the TRIP steel, the size of the austenite grains embedded in the ferritic matrix or the size of strain induced martensite in the austenitic matrix was in the order of micrometers or even more. Imaging non-magnetic austenite of a size of few nanometers in a magnetic matrix is therefore challenging, particularly in the case of very deformed surfaces from a fatigued specimen. MFM characterization was performed using a standard AFM setup (Dimension Icon, Bruker Inc., Rheinstetten, Germany) with standard CoCr coated tips (MESP-V2, Bruker Inc). MFM measurements were taken in a two-pass technique called “lift mode”. During the first pass, the topographic image was obtained by monitoring the cantilever’s oscillation amplitude changes caused by sample surface topography (tapping mode). During the second pass at a constant distance from the first pass (30–40 nm in our study), the long-range interactions were recorded via the phase change of the oscillating cantilever (phase image). At first, un-fatigued specimens polished with the same quality as for EBSD requirement were produced and analyzed by MFM. Figure 5a,b presents an overview of the same area (50 μm \times 50 μm) imaged respectively in the topographic mode and in the magnetic force mode, at a lift height of 30–40 nm. The bright and dark regions in the magnetic force image correspond to repulsive and attractive forces, respectively. A closer view in a 5 μm \times 5 μm scan (Figure 5c) points out intense repulsive force at a very fine scale which may be correlated with the austenitic nanofilms (pointed by the blue arrows).

This conclusion was supported by previous TEM observation [25]. Indeed, TEM in the imaging mode and in the Selected Area Diffraction (SAED) mode was successful in unambiguously imaging the retained austenite. This has been found in the form of very thin films, as reported in the literature [26,28], but in sufficient amounts to provide an intense diffraction spot. By selecting the right diffraction spot (Figure 6b), the dark-field images highlighted the austenite along the lath boundaries (Figure 6c).

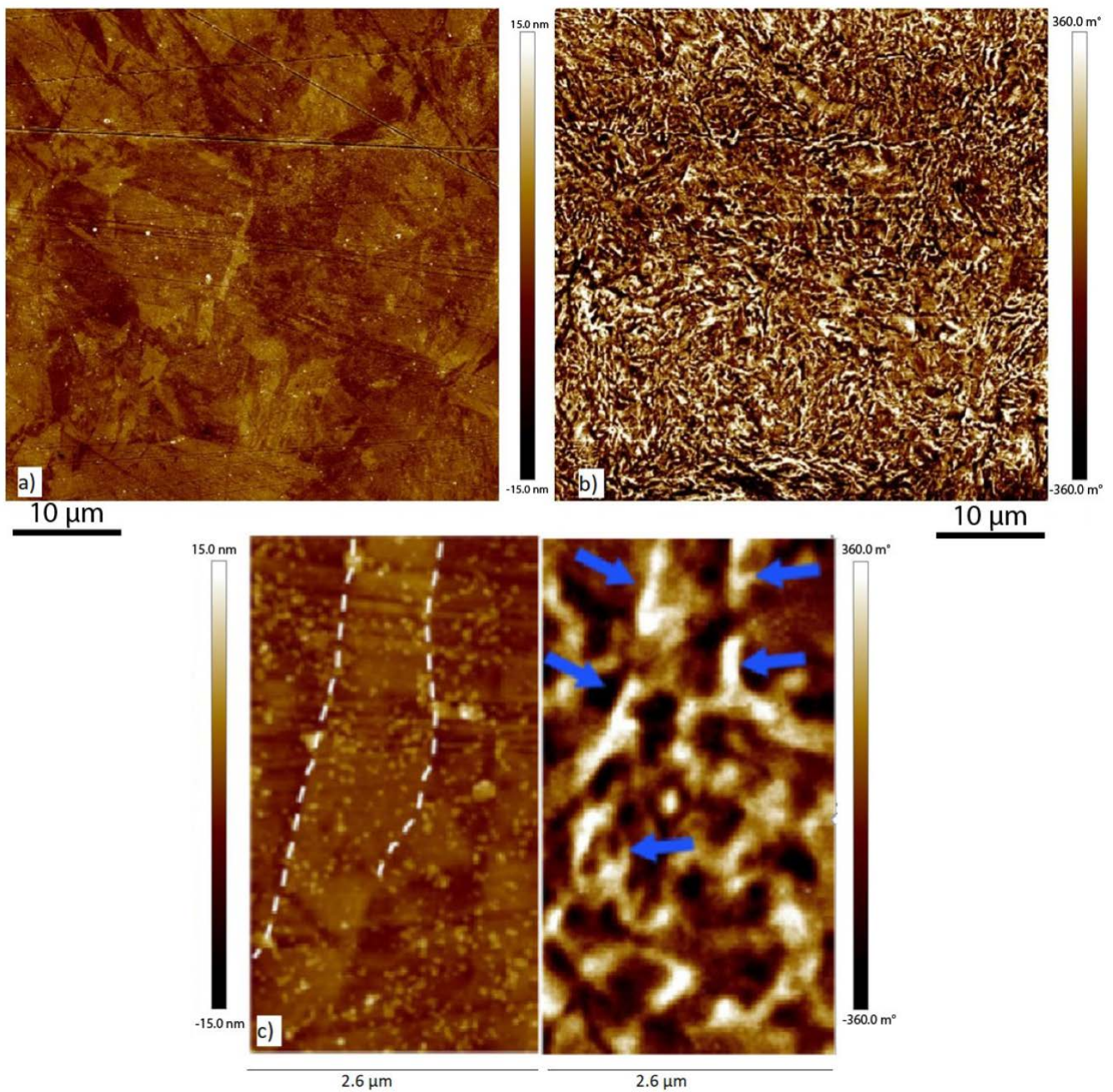


Figure 5. (a) Topographical and (b) magnetic force overview images of the same area of the non-deformed 9Ni steel and (c) identification of austenite nano-films at lath interface (dashed line).

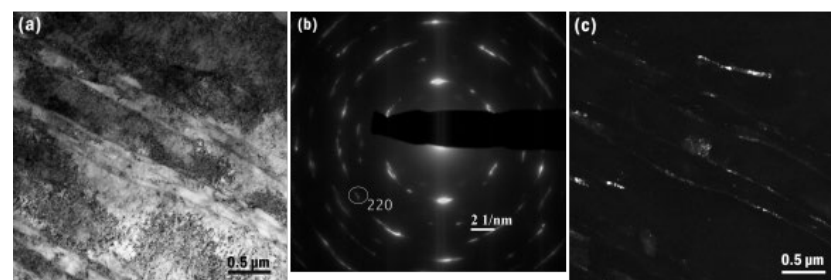


Figure 6. (a) Bright field image TEM of the unfatigued 9Ni steel, (b) Selected Area Diffraction Spot (SAED) of (220) γ , and (c) dark field image of the same area highlighting the austenitic phase. Reprinted with permission from ref. [25]. Copyright 2021 Elsevier.

Figure 7 is the surface of a specimen submitted to 80 cycles at $\Delta\epsilon_t = 1.2\%$, imaged at a high magnification in the topographical and magnetic force modes. A proper height of 80 nm was chosen to ensure that the influence of surface topography was eliminated, and the cantilever was only affected by the magnetic forces. Extrusions are visible as the brighter zones in Figure 7a. The corresponding magnetic image indicates a very light repulsive force next to some of the extrusions observed (Figure 7b).

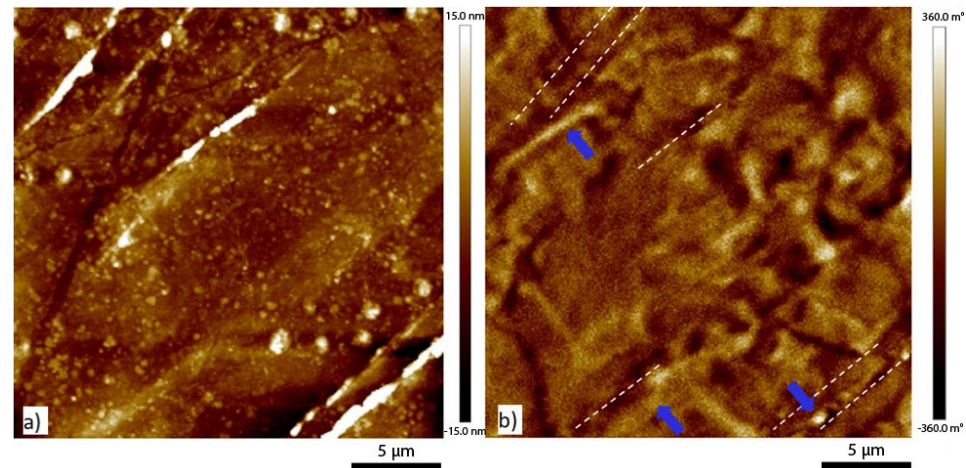


Figure 7. (a) MFM topographical image and (b) MFM magnetic force image of the quenched 9Ni steel after 80 cycles at $\Delta\epsilon_t = 1.2\%$. The blue arrow points to the austenitic phase placed next to the extrusion spotted by dashed white lines.

By superposing the images, it is possible to observe that the same repulsive bright spots are present in the vicinity of some extrusions. In some identified extrusions, no perturbation was observed, suggesting that austenite disappeared, which is consistent with XRD analysis. These observations resulting from MFM imaging allow the confirmation of extrusion formation along the retained austenite nanofilm, supporting its proposed role, namely acting as a lubricant or greasy film and thus facilitating the martensitic matter flow. On the other hand, it also confirms that retained austenite can transform upon cyclic deformation, i.e., a TRIP effect; however, this remains a very small contribution to the accommodation of the cyclic plasticity.

4. Conclusions

The present paper aimed at unambiguously explaining and understanding the surface relief formed during low cycle fatigue of a 9Ni steel. The solution heat treated and water quenched 9Ni martensitic steel indeed contains nanometric sized films of retained austenite at martensitic laths boundaries. After 80 cycles of fatigue at $\Delta\epsilon_t = 1.2\%$, fatigue intrusion–extrusion pairs formed at the surface of the specimen. Evidencing the retained austenite in the martensitic network is not problematic if it is not necessary to connect them with slip marks. The situation appeared more critical when attempting to connect the well-developed extrusions formed under cyclic plasticity with the nano-films of austenite. Using MFM and exploring the difference in magnetic properties between austenite and martensite to answer fatigue questions appeared very innovative and promising. MFM analysis associated with HRTEM images of fatigue extrusions allowed us to distinguish between the retained austenite and the extruded martensite lath. From this, the mechanism of accommodation of cyclic plasticity proposed previously is compellingly admitted. The fatigue extrusions result from a martensite matter displacement along the austenitic film which acts as a lubricant or greasy plane.

Author Contributions: Conceptualization, investigation, writing—review, M.A.C.A.; investigation, writing—draft, J.-M.O.; investigation, writing—draft, G.P.; investigation, A.A.; investigation, writing—

draft, J.B.; investigation, writing—original draft and editing, supervision, J.-B.V. All authors have read and agreed to the published version of the manuscript.

Funding: This research received no external funding.

Institutional Review Board Statement: Not applicable.

Informed Consent Statement: Not applicable.

Data Availability Statement: No data, models, or code were generated or used during the study.

Acknowledgments: The SEM and TEM national facility in Lille (France) is supported by the Conseil Regional des Hauts-de-France and the European Regional Development Fund (ERDF). One of the authors (M.A.C.A.) would like to acknowledge the partial financial support of the Roberto Rocca Education Program.

Conflicts of Interest: The authors declare that they have no known competing financial interests or personal relationships that could have appeared to influence the work reported in this paper.

References

1. Laufer, E.E.; Roberts, W.N. Dislocations and persistent slip bands in fatigued copper. *Philos. Mag.* **1966**, *14*, 65–78. [\[CrossRef\]](#)
2. Mecke, K.; Blochwitz, C. Internal displacements of persistent slip bands in cyclically deformed nickel single crystals. *Phys. Status Solidi* **1980**, *61*, K5. [\[CrossRef\]](#)
3. Cheng, A.; Laird, C. Fatigue life behavior of copper single crystals. Part I: Observations of crack nucleation. *Fat. Fract. Eng. Mater.* **1981**, *4*, 331–341. [\[CrossRef\]](#)
4. Brown, L.M. Dislocation substructures and the initiation of cracks by fatigue. *Metal Sci.* **1977**, *11*, 315–320. [\[CrossRef\]](#)
5. Kim, W.H.; Laird, C. Crack nucleation and stage I propagation in high strain fatigue—II. Mechanism. *Acta Metall.* **1978**, *26*, 789–799. [\[CrossRef\]](#)
6. Lukáš, P.; Kunz, L. Role of persistent slip bands in fatigue. *Philos. Mag.* **2004**, *84*, 317–330. [\[CrossRef\]](#)
7. Piqueras, J.; Grosskreutz, J.C.; Frank, W. The influence of point-defect clusters on fatigue hardening of copper single crystals. *Phys. Status Solidi* **1972**, *11*, 567–580. [\[CrossRef\]](#)
8. Lepistö, T.; Yli-Kaupilla, J.; Kettunen, P.; Hautofärvi, P. Voids in fatigued copper single crystals. *Phys. Status Solidi* **1981**, *67*, K93–K97. [\[CrossRef\]](#)
9. Polák, J. On the role of point defects in fatigue crack initiation. *Mater. Sci. Eng.* **1987**, *92*, 71–80. [\[CrossRef\]](#)
10. Ho, H.S.; Risbet, M.; Feaugas, X.; Favergeon, J.; Moulin, G. Fundamental mechanisms of surface damage associated to the localization of the plastic deformation in fatigue. *Proc. Eng.* **2010**, *2*, 751–757. [\[CrossRef\]](#)
11. Hu, Y.; Chen, Y.; He, C.; Liu, Y.; Wang, Q.; Wang, C. Bending Fatigue Behavior of 316L Stainless Steel up to Very High Cycle Fatigue Regime. *Materials* **2020**, *13*, 4820. [\[CrossRef\]](#)
12. Salazar, D.; Serre, I.; Vogt, J.-B. LCF mechanisms of the 25Cr-7Ni-0.25N duplex stainless steel investigated by atomic force microscopy. In Proceedings of the Sixth International Conference on Low Cycle Fatigue (LCF 6), Berlin, Germany, 8–12 September 2008; DVM: Berlin, Germany, 2008; pp. 85–90.
13. Ma, B.T.; Laird, C. Overview of fatigue behavior in copper single crystals—I. Surface morphology and stage I crack initiation sites for tests at constant strain amplitude. *Acta Metall.* **1989**, *37*, 325–336. [\[CrossRef\]](#)
14. Basinski, Z.S.; Basinski, S.J. Low amplitude fatigue of copper single crystals—III. PSB sections. *Acta Metall.* **1985**, *33*, 1319–1327. [\[CrossRef\]](#)
15. Höppel, H.; Goik, P.; Krechel, C.; Göken, M. Ex and in situ investigations on the role of persistent slip bands and grain boundaries in fatigue crack initiation. *J. Mater. Res.* **2017**, *32*, 4276–4286. [\[CrossRef\]](#)
16. Man, J.; Vystavěl, T.; Weidner, A.; Kuběna, I.; Petreenc, M.; Kruml, T.; Polák, J. Study of cyclic strain localization and fatigue crack initiation using FIB technique. *Int. J. Fatigue* **2012**, *39*, 44–53. [\[CrossRef\]](#)
17. Essmann, U.; Gösele, U.; Mughrabi, H. A model of extrusions and intrusions in fatigued metals I. Point-defect production and the growth of extrusions. *Philos. Mag. A* **1981**, *44*, 405–426. [\[CrossRef\]](#)
18. Hunsche, A.; Neumann, P. Quantitative measurement of persistent slip band profiles and crack initiation. *Acta Metall.* **1986**, *34*, 207–217. [\[CrossRef\]](#)
19. Polak, J.; Man, J. Mechanisms of extrusion and intrusion formation in fatigued crystalline materials. *Mater. Sci. Eng. A* **2014**, *596*, 15–24. [\[CrossRef\]](#)
20. Polák, J. Role of Persistent Slip Bands and Persistent Slip Markings in Fatigue Crack Initiation in Polycrystals. *Crystals* **2023**, *13*, 220. [\[CrossRef\]](#)
21. Polak, J.; Mazanova, V.; Heczko, M.; Kunena, I.; Man, J. Profiles of persistent slip markings and internal structure of underlying persistent slip bands. *Fatigue Fract. Eng. Mater. Struct.* **2017**, *40*, 1101–1116. [\[CrossRef\]](#)
22. Krupp, U.; Giertler, A. Surface or Internal Fatigue Crack Initiation during VHCF of Tempered Martensitic and Bainitic Steels: Microstructure and Frequency/Strain Rate Dependency. *Metals* **2022**, *12*, 1815. [\[CrossRef\]](#)

23. Wildeis, A.; Christ, H.-J.; Brandt, R. Influence of Residual Stresses on the Crack Initiation and Short Crack Propagation in a Martensitic Spring Steel. *Metals* **2022**, *12*, 1085. [[CrossRef](#)]
24. Seidametova, G.; Vogt, J.-B.; Proriol Serre, I. The early stage of fatigue crack initiation in a 12%Cr martensitic steel. *Int. J. Fatigue* **2018**, *106*, 38–48. [[CrossRef](#)]
25. Cota Araujo, M.A.; Vogt, J.-B.; Bouquerel, J. Retained austenite-aided cyclic plasticity of the quenched 9Ni steel. *Int. J. Fatigue* **2021**, *152*, 106445. [[CrossRef](#)]
26. Maresca, F.; Kouznetsova, V.G.; Geers, M.G.D. On the role of interlath retained austenite in the deformation of lath martensite. *Model. Simul. Mater. Sci. Eng. A* **2014**, *22*, 045011. [[CrossRef](#)]
27. Cullity, B.D. *Elements of X-ray Diffraction*; Addison-Wesley Publishing: Boston, MA, USA, 1956.
28. Morito, S.; Oh-Shi, K.; Hono, T.; Ohba, T. Carbon enrichment in retained austenite films in low carbon lath martensite steel. *ISIJ Int.* **2011**, *51*, 1200–1202. [[CrossRef](#)]
29. Zhang, Z.; Delagne, D.; Bernhard, G. Ageing effect on cyclic plasticity of a tempered martensitic steel. *Int. J. Fatigue* **2007**, *29*, 336–346. [[CrossRef](#)]
30. Jürgens, M.; Olbricht, J.; Fedelich, B.; Skrotzki, B. Low Cycle Fatigue and Relaxation Performance of Ferritic–Martensitic Grade P92 Steel. *Metals* **2019**, *9*, 99. [[CrossRef](#)]
31. Kanetani, K.; Moronaga, T.; Hara, T.; Ushioda, K. Deformation-Induced Martensitic Transformation Behavior of Retained Austenite during Rolling Contact in Carburized SAE4320 Steel. *ISIJ Int.* **2021**, *61*, 2629–2635. [[CrossRef](#)]
32. Ke, X.; Zhang, M.; Zhao, K.; Su, D. Moiré fringe method via scanning transmission electron microscopy. *Small Method* **2022**, *6*, 2101040. [[CrossRef](#)]
33. Fultz, B.; Kim, J.I.; Kim, Y.H.; Fior, G.O.; Morris, J.W. The stability of precipitated austenite and the toughness of 9Ni steel. *Metall. Mater. Trans. A* **1985**, *16*, 2237–2249. [[CrossRef](#)]
34. Passeri, D.; Dong, C.; Reggente, M.; Angeloni, L.; Barteri, M.; Scaramuzza, F.A.; De Angelis, F.; Marinelli, F.; Antonelli, F.; Rinaldi, F.; et al. Magnetic force microscopy: Quantitative issues in biomaterials. *Biomatter* **2014**, *4*, e29507. [[CrossRef](#)] [[PubMed](#)]
35. Vokoun, D.; Samal, S.; Stachiv, I. Magnetic Force Microscopy in Physics and Biomedical Applications. *Magnetochemistry* **2022**, *8*, 42. [[CrossRef](#)]
36. Gadelrab, K.R.; Li, G.; Chiesa, M.; Souier, T. Local characterization of austenite and ferrite phases in duplex stainless steel using MFM and nanoindentation. *J. Mater. Res.* **2012**, *27*, 1573–1579. [[CrossRef](#)]
37. Zens, A.S.; Appel, T.; Broekaert, J.A.C.; Friedel, F. Determination of retained austenite in multiphase steels by magnetic force microscopy. *Int. J. Mater. Res.* **2006**, *97*, 1158–1162. [[CrossRef](#)]
38. Shen, L.Q.; Luo, P.; Hu, Y.C.; Bai, H.Y.; Sun, Y.H.; Sun, B.A.; Liu, Y.H.; Wang, W.H. Shear-band affected zone revealed by magnetic domains in a ferromagnetic metallic glass. *Nat. Commun.* **2018**, *9*, 4414. [[CrossRef](#)]

Disclaimer/Publisher’s Note: The statements, opinions and data contained in all publications are solely those of the individual author(s) and contributor(s) and not of MDPI and/or the editor(s). MDPI and/or the editor(s) disclaim responsibility for any injury to people or property resulting from any ideas, methods, instructions or products referred to in the content.